This item is the archived peer-reviewed author-version of:

Insights into the reactivity properties, docking, DFT and MD simulations of orphenadrinium dihydrogen citrate in different solvents

Insights into the reactivity properties, docking, DFT and MD simulations of orphenadrinium dihydrogen citrate in different solvents

Jamelah S.Al-Otaibi[a*], Y.Sheena Mary[b], Y.Shyma Mary[b], Sanja J. Armaković[c,e], Stevan Armaković[d,e], Christian Van Alsenoy[f], H.S.Yathirajan[g]

[a] Department of Chemistry, College of Science, Princess Nourah Bint Abdulrahman University, P.O. Box 84428, Riyadh 11671, Saudi Arabia
[b] Thushara, Neethinagar-64, Pattathanam, Kollam, Kerala, India
[c] University of Novi Sad, Faculty of Sciences, Department of Chemistry, Biochemistry and Environmental Protection, 21000 Novi Sad, Serbia
[d] University of Novi Sad, Faculty of Sciences, Department of Physics, 21000 Novi Sad, Serbia
[e] Association for the International Development of Academic and Scientific Collaboration (AIDASCO), 21000 Novi Sad, Serbia
[f] Structural Chemistry Group, Department of Chemistry, University of Antwerp, Groenenborgerlaan 171, B-2020, Antwerp, Belgium
[g] Department of Studies in Chemistry, University of Mysore, Manasagangotri, Mysore, Karanataka, India

*author for correspondence: jamelah2019@rediffmail.com

Abstract
Experimental and theoretical investigations of a novel compound, Orphenadrinium dihydrogen citrate (ODC) are reported. Wavenumbers are assigned by means of vibrational spectroscopy. The stability in solvents was tested by adding water, DMSO, and methanol to different solvent models. The solvation energies are -21.65 (acetone), -22.49 (DMSO) and -22.76 (water) kcal/mol and are found to be good solvents for the ODC. ODC is more compact within DMSO and not compact in water and methanol in the period of 100 ns. RMSF analysis shows destabilization of the protein. MD simulations were performed to calculate the radial distribution functions to identify the most critical interactions with water molecules. MD simulations were also applied to obtain the temperature dependence of density. Analyzing the electron density between all atoms, noncovalent interactions between fragments have been identified and quantized.
Keywords: Orphendrine; DFT; MD simulations; Solvent effects; Non-covalent interactions

Introduction
        Orphenadrine citrate belongs to the ethanolamine antihistamine class of skeletal muscle relaxants. It is used to treat muscle injuries that require physiotherapy, such as strains and sprains, as well as Parkinson's disease, where it helps with motor control. It can also be used to treat rheumatoid arthritis [1]. Orphenadrine is beneficial for pain of many etiologies due to its anticholinergic actions and central nervous system penetration [2]. Orphenadrine is structurally similar to diphenhydramine and has characteristics than diphenhydramine. It is primarily eliminated through kidneys [3]. As a result, its potential for testing in the treatment of muscle cramps caused by liver cirrhosis appears rational [4, 5]. A few clinical researches on the effects of orphenadrine and paracetamol on myalgia found that the pain relieving effect

was boosted [6]. Orphenadrine citrate is commonly used in conjunction with paracetamol [7]. An ethanamine derivative has recently been reported as a possible antibiotic against staphylococcus aureus [8]. Jeyashri et al. reported the design, synthesis and DFT analysis of pyrrolidine-ethanamine derivatives [9]. Ethanamine derivatives are powerful serotonin receptor agonist that has psychological and behavioral consequences [10, 11]. Terrazasl-Lopez et al reported the interaction of orphenadrine with desuccinylase recently [12]. Orphendrine is an antihistamine with anticholinergic properties that was first used to treat muscular discomfort and wound pain, as well as to manage Parkinsons disease [13]. It is regarded as a dirty drug since its activity is mediated by a variety of molecular targets [14]. Antihistamine drugs have been found to be effective antibacterial agents [15-17]. Escudero et al reported dihydrogen citrate derivative in aqueous solution of triton surfactants [18]. Due to its well-known biocompatibility and natural presence in human body, dihydrogen citrate anion is a suitable contender [19]. Shah et al reported the femtomolar detection of orphenadrine using nanostructure based electrochemical sensor [20]. According to a review of the literature, no complete quantum mechanical calculation for Orphenadrinium dihydrogen citrate (ODC) has yet been published. Drug design and research in vibrational spectroscopy rely heavily on quantum chemical computations and molecular modeling [21, 22]. The XRD study of the ODC is reported by Kaur et al. [23]. The quantum chemistry theory, DFT, molecular models and vibrational spectroscopy are heavily used in drug research and development [24]. Docking studies reveal the interaction and binding of ligands with receptors as well as drug's mechanism of action [25]. MD simulations can display the oscillations of receptors and ligands to help understand the function of medicines and proteins [26]. Therefore, docking using MD simulations can be used to thoroughly and methodically analyze the structural characteristics and binding mechanism of ligands and receptors. In addition to reactivity analyses, MD simulations, DFT investigations of ODC provide additional information regarding their electronic, structural and reactivity properties. DFT is additionally utilized to obtain the most accurate outcome of ODC characteristics in a selection of eco-solvents [27]. Solvents have a wide range of applications, including the chemical and pharmaceutical sectors. Solvents can influence reaction speed and stability. Non-polar and polar liquids can both be used as solvent for the title molecule. Methanol and DMSO are widely used as dissolving agents to screen the pharmaceutical properties [28]. Hence in the present study, polar aprotic DMSO, acetone and polar protic water are taken as the solvents. NBO analysis is used to determine the chemical drug's stability. MEP investigations identify the reactive sites and FMO analysis gives stability, energy gap etc. Docking together with MD simulations was used to determine the biological activity of ODC by determining drug likeness, ligand interactions and appropriate protein interactions.
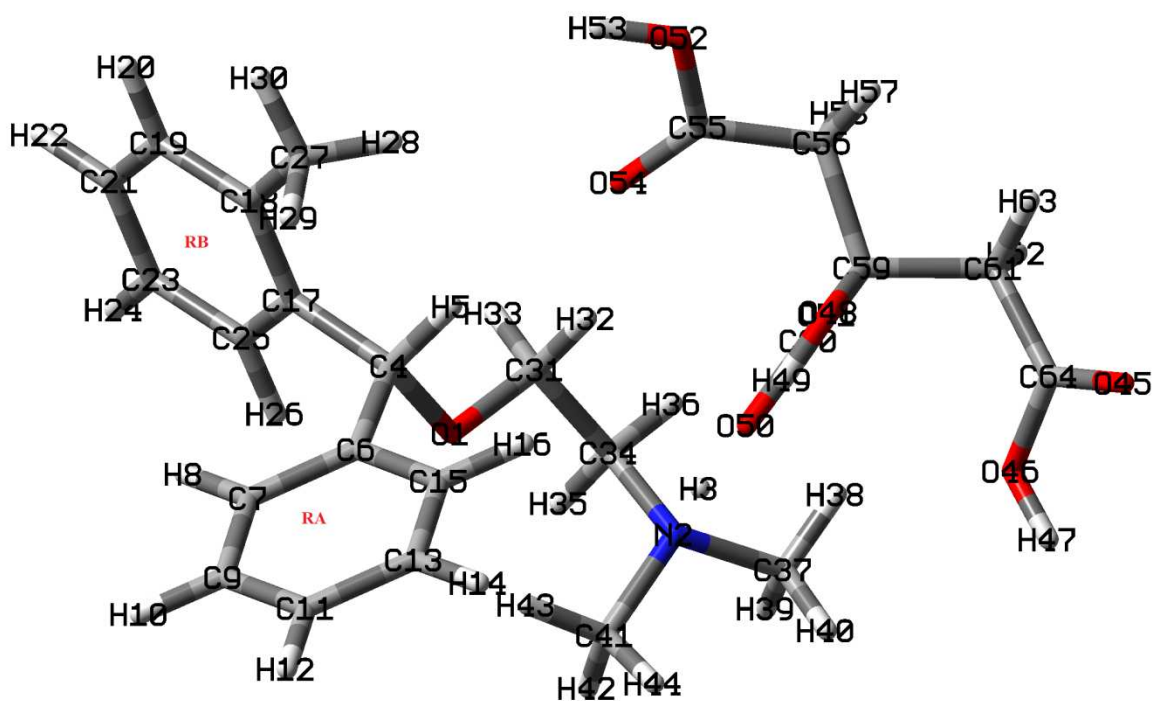
Methods

Figure 1. Optimized structure of Orphenadrinium dihydrogen citrate (ODC)

ODC was obtained as a gift sample from Kaur et al. [23] and the vibrational spectra are given in Fig.S1 and Fig.S2. The Gaussian 16 package and GaussView, Version 6.1 were used to determine the characteristics of ODC [29, 30]. Using B3LYP/6-311++G* basis set, DFT was utilized to optimize ODC (Fig.1). ODC was docked into the active site of carbidopa inhibitor 1JS3, which has been linked to a range of clinic problems [31]. For simulation purposes, a system was set up to include protein alone (1JS3) and 1JS3-ODC complex with solvent [32, 33]. The OPLS force field was added to the system and SPC water system. The stability of ODC in different solvents was tested by adding water, DMSO, and methanol to different solvent models (100 ns simulations) and for 1JS3-ODC complex MD simulation is run for a period of 150ns for getting properties like, RMSD, RMSF, Rg and H-Bond data. The Desmond program version 2022-1 [33-37], was also used along with the OPLS4 force field for a simulation time of 10 ns [38-41], to investigate the influence of water. These MD simulations allowed us to consider the influence of water explicitly. Quantum-mechanical calculations based on the DFT to obtain MEP, ALIE, and noncovalent interactions were performed with the Jaguar [34, 35] program, also as incorporated in the SMSS [42-45]. Binding energies between ODC and CIT fragments have been calculated according to the following equation: $E_B = E(ODC) - E(ORP) - E(CIT)$ where $E(ODC)$ stands for the total energy of the complex, $E(ORP)$ stand for the total energy of the ORP fragment, $E(CIT)$ stands for the total energy of the CIT fragment. To avoid the basis set superposition error (BSSE) when calculating the binding energies, a B3LYP-MM [46] functional was applied. This is a posteriori-corrected functional that has been parametrized over a huge set of complexes with noncovalent interactions. B3LYP-MM automatically includes the counterpoise correction,

necessary to take into account the BSSE, so no further activities are required to obtain reliable binding energies.

Binding energies between fragments have been obtained considering different solvents as well. In cases when solvent effects were considered for calculations of binding energies, an implicit method based on the Poisson-Boltzman solver [47] was applied, as incorporated in the Jaguar program for quantum mechanical calculations.

Results and discussion

Vibrational spectra

The phenyl ring modes (table S1) are at: 3049 (IR), 3067-3031 (DFT) (υCH); 1310 (IR), 1577-989 (DFT) (υRA); 1356, 1017 (IR), 1354-1015 cm^{-1} (DFT) (δCH); 948, 920 (IR), 991-850 cm^{-1} (DFT) (γCH) for mono-substituted ring RA and at 3085, 3026 (IR), 3068, 3042, 3026 (Raman), 3068-3028 (DFT) (υCH), 1580, 1545, 1032 (IR), 1580, 1030 (Raman), 1578-1031 cm^{-1} (DFT) (υRB); 1285, 1055 (IR), 1100 (Raman), 1282-1053 (DFT) (δCH); 985-746 cm^{-1} (DFT) (γCH) for the 1,2-substitued ring RB [48].

The CH$_3$ modes are at: 2943, 2895 (IR), 2918 (Raman), 3051-2893 cm^{-1} (DFT) (υCH3) and at 1475, 1456, 1425, 1222, 1146 (IR), 1467, 1420, 1071 (Raman), 1492-1070 cm^{-1} (DFT) (δCH$_3$). The CH$_2$ modes are at: 2995, 1966, 2870 (Raman), 3005-2884 cm^{-1} (DFT) (υCH$_2$) and at 1390, 1310, 1241, 1198, 1105, 928, 858, 828 (IR), 1486, 1444, 1388, 1340, 1307, 1290, 1236, 1197, 927, 859, 830 (Raman), 1485-773 cm^{-1} (DFT) (δCH$_2$) [48]. The CO stretching modes are assigned at: 1640, 1632, 1505, 1439 (C=O) and at 1316, 1295, 1041, 962 cm^{-1} (C-O) which are observed at 1645, 962 in IR and at 1290, 1044 cm^{-1} in Raman spectra [48, 49]. The υOH modes are at 3434 (IR), 3230 (Raman) and at 3495, 3490, 3366 cm^{-1} theoretically [48]. The NH…O modes are assigned at 2155 (IR), 2145, 1600 (Raman) and at 2174, 1767, 1603 cm^{-1} (DFT) as expected [48].
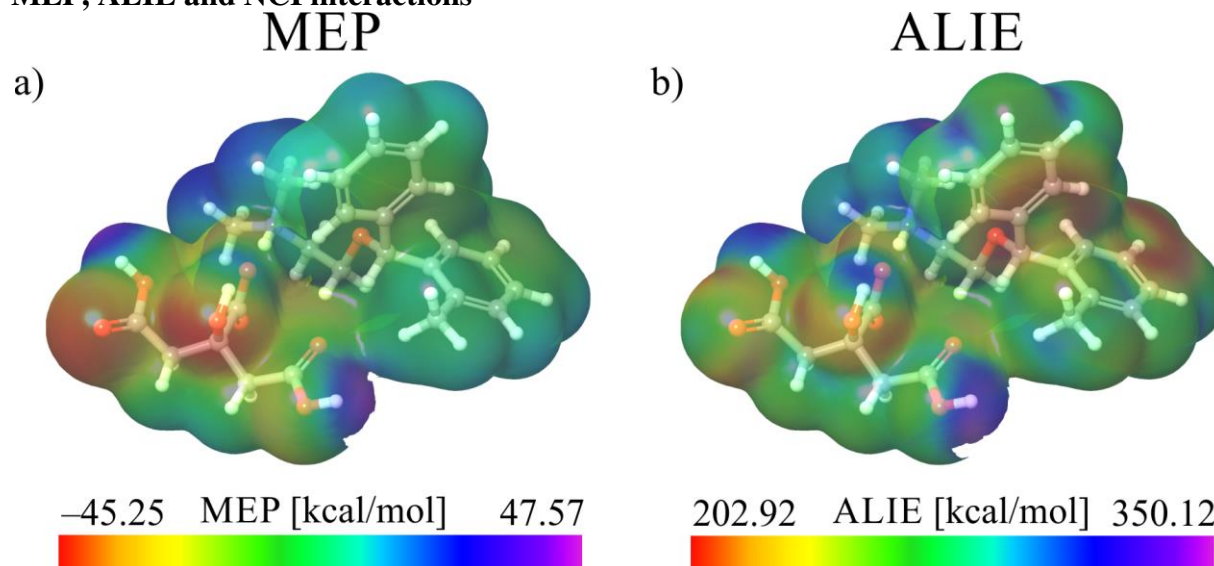
MEP, ALIE and NCI interactions

Figure 2. a) MEP and b) ALIE surfaces of the ODC system

MEP and ALIE descriptors were employed to identify characteristic reactive sites of ODC. These descriptors were presented in the forms of electron density surfaces mapped with the values of MEP and ALIE obtained via DFT calculations. The obtained color-schemed surfaces are easily analyzed with the aim of identifying sites with the highest and lowest

values of mentioned descriptors. The obtained MEP and ALIE surfaces (Figure 2) indicate that the citrate (CIT) fragment bears higher electron density, as the lowest MEP values are mainly localized at its oxygen atoms. The lowest and highest MEP values reach -45.0 and 47.57 kcal/mol and are localized at both CIT and orphenadrinium (ORP) fragments. Although the higher electron density characterizes the CIT fragment, the ORP fragment is characterized by the lower ALIE values (red-colored in Figure 2(b)), indicating that it is more sensitive to the electrophilic attacks. To a certain extent, low ALIE values are distributed again around the oxygen atoms of the CIT fragment; however, to a much greater extent, these ALIE values are distributed near to benzene rings of the ORP fragment [50, 51].
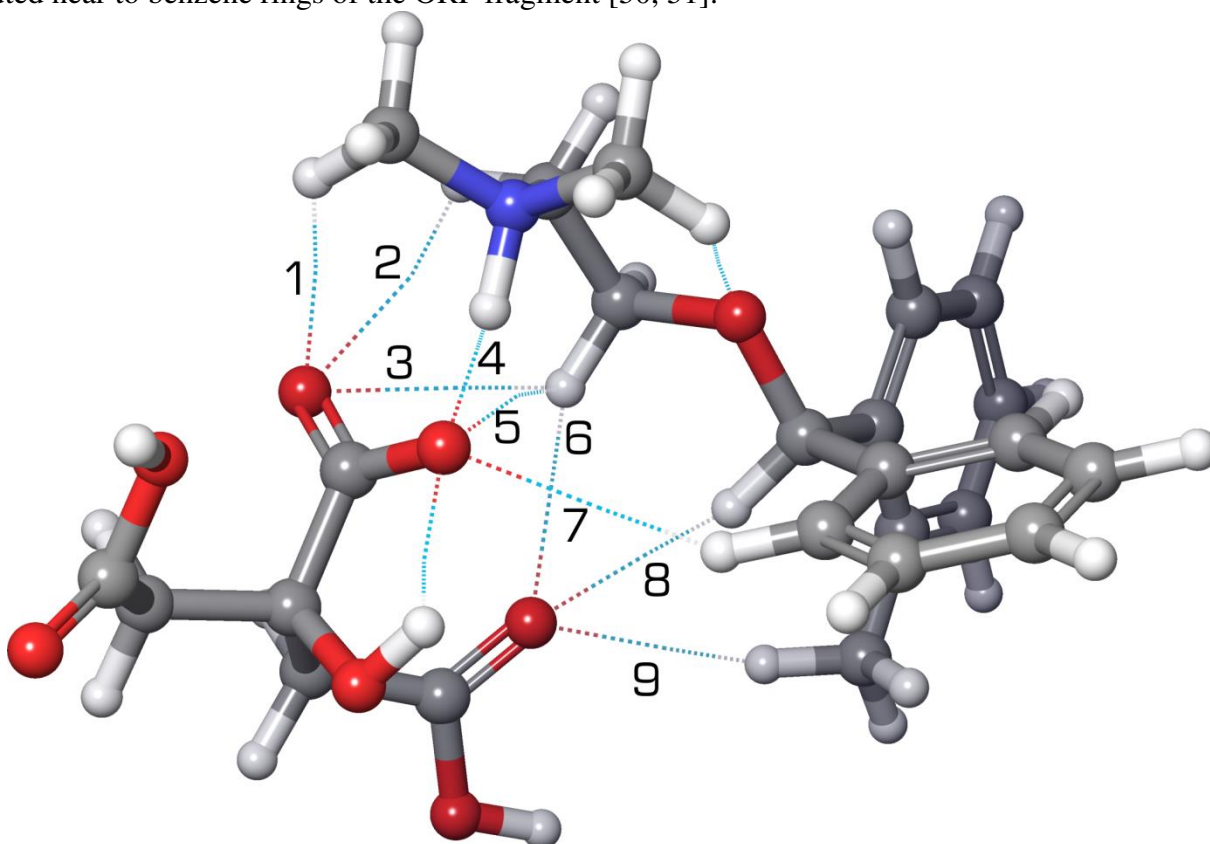

Figure 3. Noncovalent interactions of the ODC system

Table 1. Strengths (in electron density) of intermolecular noncovalent interactions

NCI	NCI strength	NCI	NCI strength
1	-0.0110	6	-0.0077
2	-0.0057	7	-0.0027
3	-0.0052	8	-0.0081
4	-0.0782	9	-0.0056
5	-0.0065	-	-

In Figure 3 and Table 1, all intermolecular NCI and the strengths have been enumerated. The study of electron density to reveal noncovalent interactions is based on

identifying the bond critical points, which are the points where the electron density is minimal at certain point on the line that connects two atoms, and in the same time it is maximal with respect to the both directions perpendicular to the bond. The procedure is to identify these bonds, noncovalent interactions and their corresponding strengths. The results presented in Figure 3 indicate that a large number of NCI form between CIT and ORP fragments. Namely, the total number of 9 NCI form, of which the strongest is certainly the NCI denoted with the number 4. In this case, the strength of the NCI is equal to -0.0782 and is formed between the hydrogen atom of ORP's NH group and the oxygen atom of the CIT's carboxyl group. The second strongest NCI is formed between the hydrogen atom of the ORP's methyl group and the same CIT's carboxyl group. All other NCIs have at least one order of magnitude weaker strengths [52, 53].
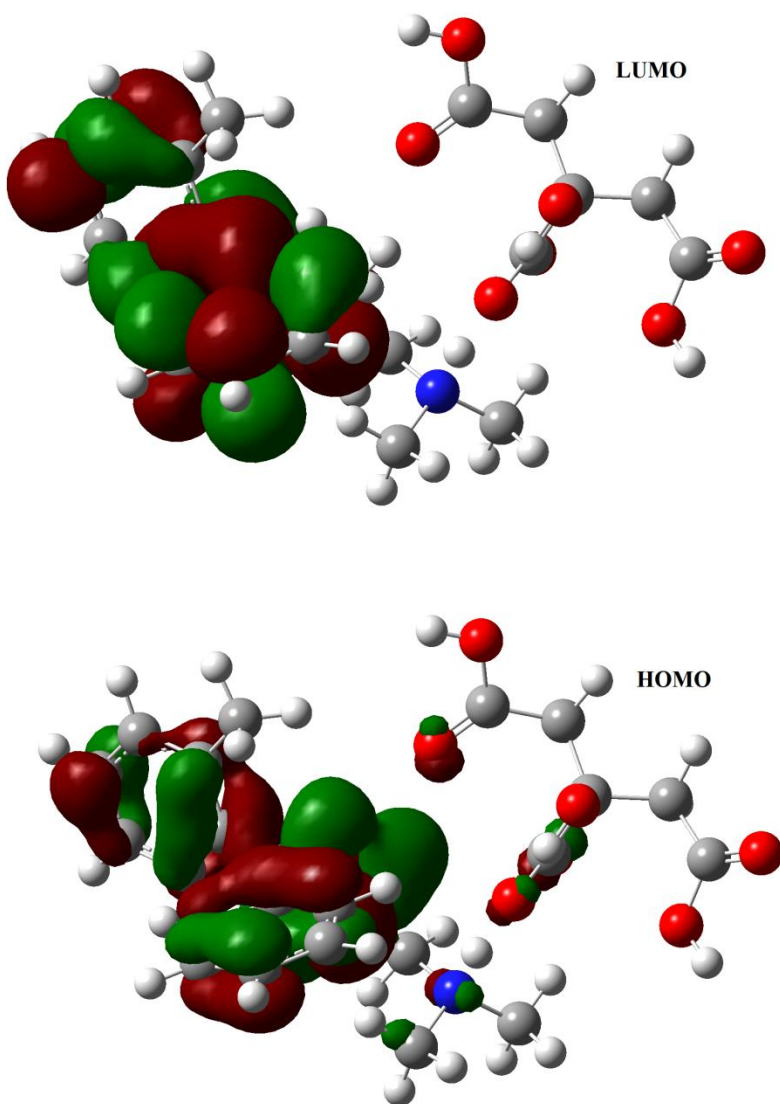
Electronic and chemical properties

Figure 4. HOMO-LUMO plots of Orphenadrinium dihydrogen citrate (ODC)

In quantum chemistry, the energy band gap and the FMOs (Fig.4) are important because they help to describe a molecule's reactivity and stability [54]. The lower the energy, the easier to excite a molecule's electrons and energy gap is a measure of excitability of molecule. Because a bigger energy gap shows stability, it is an important stability measure. The molecule's chemical and biological activity has been determined by both energy gap and their orbitals involved and ODC's energy gap is 5.8256 eV. The localized orbitals of FMOs are dispersed over phenyl rings, which clearly describe the molecular charge transfer. The FMOs energy was used to calculated reactivity descriptors [55]. The reactivity descriptors as calculated as, η = 2.9128, = -3.7958 and ω = 2.4732 eV. The ODC was classified as a stable due to its narrow gap and hardness [56].

Table 2. Influence of different solvents on dipole moment, polarizability, solvation and binding energies

| ODC in	Dipole moment (Debye)	Polarizability (a.u.)	Solvation energy (kcal/mol)	Binding energy (kcal/mol)
Vacuum	7.04	312.41	-	-123.80
Water	10.63	415.15	-22.76	-119.75
Acetone	10.34	409.91	-21.65	-123.06
DMSO	10.58	413.90	-22.49	-120.26

Because polarity differences can produce considerable changes in the relative energy in solution, solvent effects are crucial in stability phenomena [57]. The ODC molecule is re-optimized at the same level of theory in different aqueous media in order to quantify the effects of aqueous environment: polar aprotic DMSO (ε =46.68) and acetone (ε= 20.493) and polar protic water (ε =80.10). The solvation energies are found to be -21.65, -22.49 and -22.76 kcal/mol for the solvents, acetone, DMSO and water, respectively and are found to be good solvents for the ODC. By raising the polarity of the solvent and switching from gas to solution phases, the dipole moments are raised. As a result, increase stability in polar solvents containing an electron donating group could be linked to an increase in dipole moments (table 2). The polarizability of ODC is 312.41 au which increase to 409.91, 413.90 and 415.15 au in the solvents, acetone, DMSO and water, which means there is an enhancement of NLO property in solvent media. The values of energy gap and hardness decrease in solvent media while the chemical potential becomes more negative in solvent media. The increase in electrophilicity index in solvent media is evident for the reactivity changes.

The solvents also influenced the binding energies between the ORP and CIT fragments. In the vacuum, the binding energy was calculated to -123.80 kcal/mol, which was considered to be very strong. However, this is expected since both constituting fragments of ODC contain unpaired electrons, leading to high reactivity. The lowest binding energy was calculated when the effects of water as a solvent were taken into account (-119.75 kcal/mol). The highest binding energy with the solvent was in the case of acetone, when the calculations lead to the value of -123.06 kcal/mol just slightly lower than in the vacuum. The effects of DMSO were similar to acetone since the binding energy lowered to -120.06 kcal/mol compared to the vacuum case.

The stronger interactions due to NBO interactions are from O atoms of OH groups as [58, 59]: $n_1(O_{46}) \rightarrow \sigma^*(O_{45}-C_{64})$ and $n_1(O_{52}) \rightarrow \pi^*(O_{54}-C_{55})$ with stabilization energies 42.63 and 42.87kcal/mol respectively. Also other major interactions due to lone pair atoms are: $n_1(O_{45}) \rightarrow \sigma^*(O_{46}-C_{64})$, $n_1(O_{51}) \rightarrow \sigma^*(O_{50}-C_{60})$ and $n_1(O_{54}) \rightarrow \sigma^*(O_{52}-C_{55})$ with energies, 34.16, 20.92 and 32.13 kcal/mol. From ODC, 100% p-character was found in n_2O_{45}, n_2O_{48}, n_2O_{54}, n_2O_1, n_2O_{46}, n_2O_{51} and n_2O_{52} atoms.

Molecular dynamics simulations with solvents and docking

MD simulations aid in the understanding of ligand behavior in various solvents. During the simulation, the structure of ODC was subjected to RMSD. Higher fluctuation during MD simulation suggests molecular instability, while smaller fluctuation shows strong biological system stability. Figure 5a shows the RMSD plots of water, DMSO and methanol across the simulation duration. There were no major fluctuations, and the average RMSD was 2.67Å with DMSO. This suggests that the ligand of choice is more stable in DMSO. In solvated system, the ODC atoms have stability, compactness, reduced structural fluctuations and ODC-solvent interactions despite the greater average RMSD relative to other solvents. There was higher divergence in the case of water and methanol, indicating that the selected ligand was not stable in water and methanol during a 100 ns period. In the case of methanol and water, the average RMSD was 4.92 and 3.94Å, respectively. The compactness of ODC molecules was calculated using the Radius of gyration (Rg) method (Fig.5b). There was no substantial fluctuation, and an average Rg of 4.40 was found. This shows that ODC is more compact in DMSO. There was less compact in water and methanol, indicating that ODC was not compact in these solvents over a 100 ns period. In the case of methanol and water, the average Rg was 6.92 and 5.77 [60].
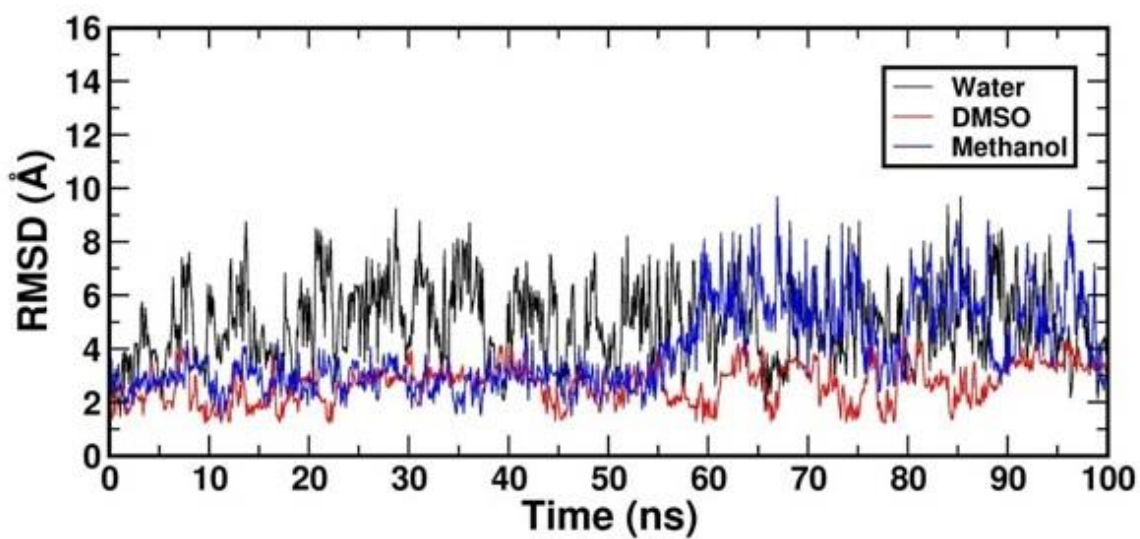
(a)
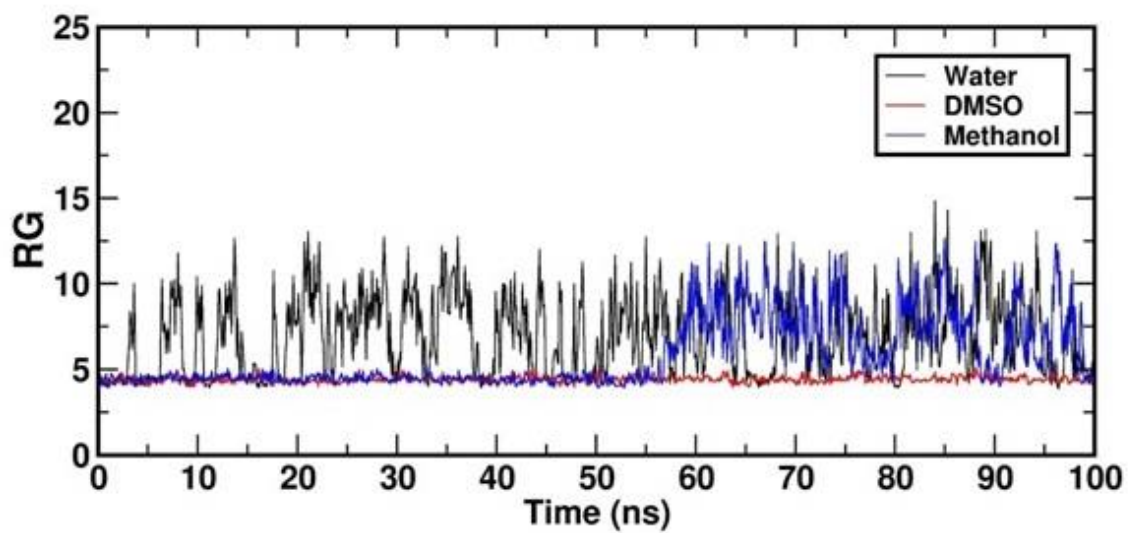
(b)

Figure 5. (a) RMSD (b) Rg plots of Orphenadrinium dihydrogen citrate (ODC) in solvents
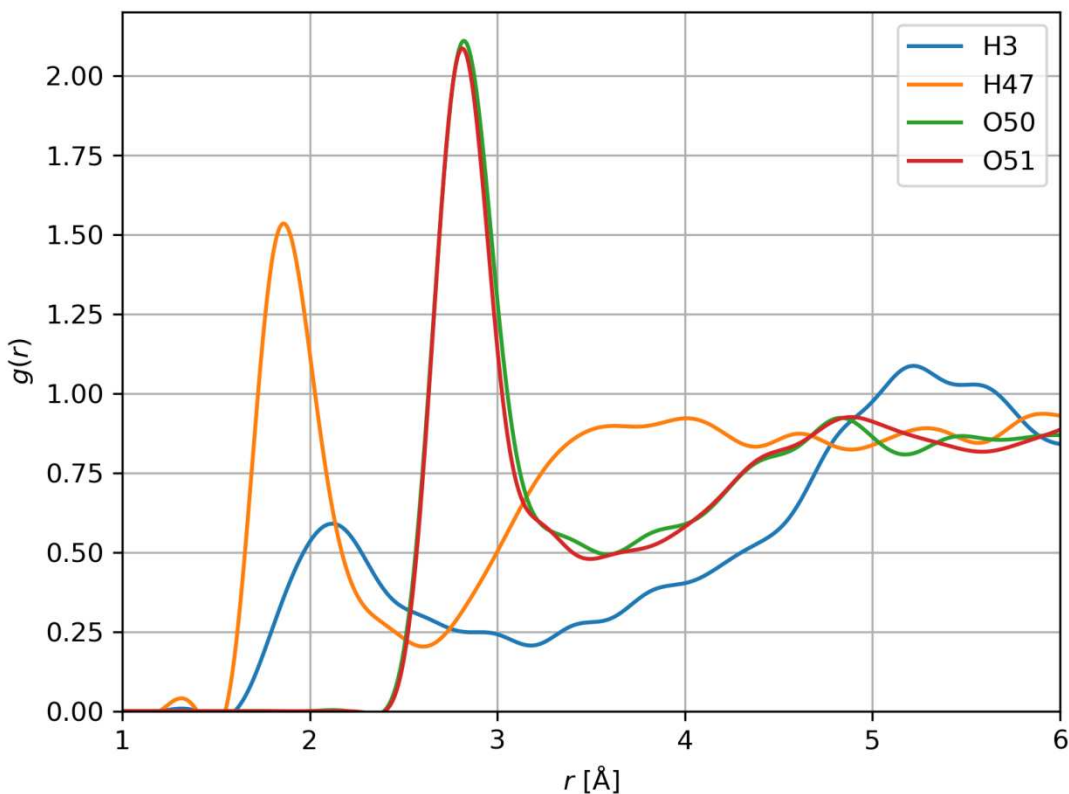
Figure 6. Representative RDFs of ODC system

Among other results, MD simulations were used to identify which atoms of the ODC system have significant interactions with water, through calculations of RDF. RDF has been calculated by taking the distance between atoms of the ODC and oxygen atom of the water molecules that surround the ODC system. Figure 6 contains representative RDFs of the ODC system. To obtain RDFs, MD system that was used consisted of one ODC system surrounded by approximately 2000 water molecules. Results in Figure 6 indicate that the ODC system has at least three atoms with considerable interactions with water. Namely, the RDF characterized by the lowest distance is the one corresponding to the H47 atom. In this case, the highest $g(r)$ value is located at the distance well below 2 Å, giving the strong interactions between H47 and water molecules. One more hydrogen atom H3 also has significant interactions. In this case, the maximal $g(r)$ value is low, but still it is locate at the distance somewhat higher than 2 Å. O50 and O51 atoms have even higher $g(r)$ values, however, the distances at which these peaks are located are much higher than in case of the H47. Nevertheless, these distances are well below 3 Å, again indicating that these two atoms also have interactions with water molecules.

To study the temperature dependence of density, one more MD system was considered. That is the MD system consisting of 32 ODCs in a cubic simulation box that was run under the same conditions as the MD system for studying interactions with water. This system was run for a series of MD simulations in a temperature range from 273 to 373 K in steps of 10 K. For each temperature, the density was calculated (Figure 7) and the temperature

dependence of density is dynamics, probably owing to the changes in interaction between CIT and ORP fragments at different temperatures. Namely, until 303 K, there is a somewhat small increase in the density, followed by a sudden drop in the range between 323 and 343 K. This sudden drop is followed by one more increase from 343 K to 353 K.
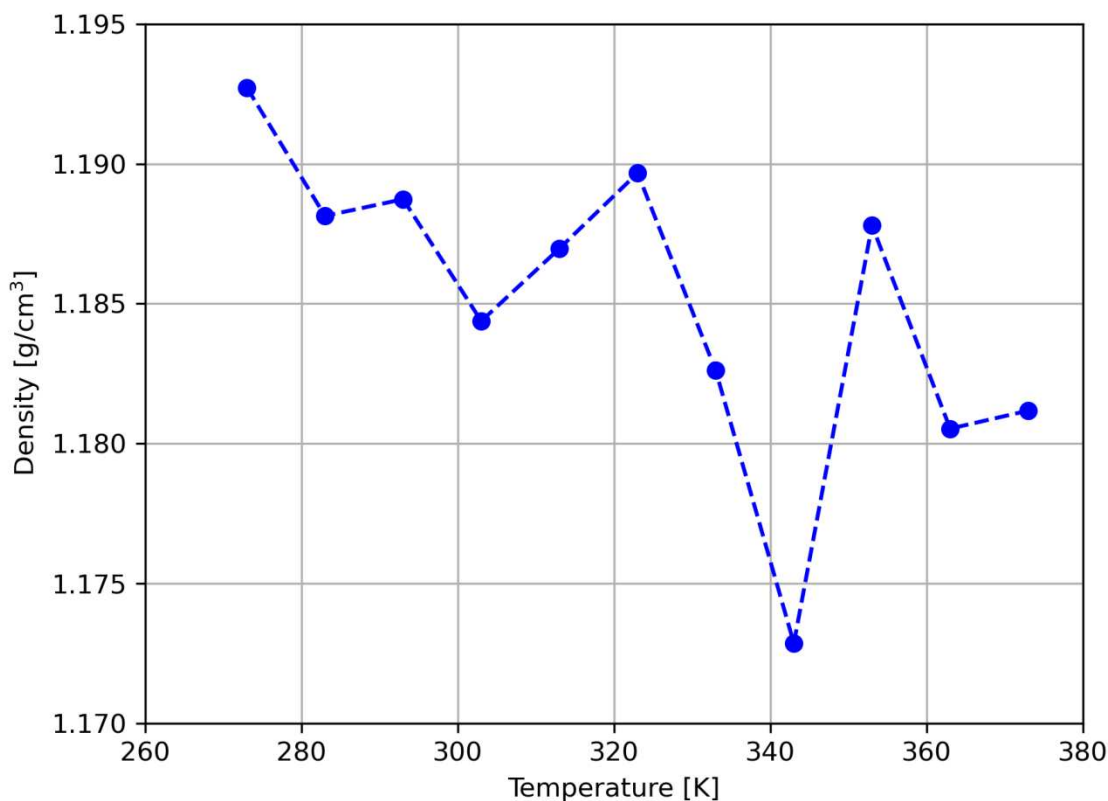

Figure 7. Temperature dependence of density for ODC system

The drop in density at 323 K may be considered by analyzing the noncovalent interactions again. Namely, there is fairly large number of noncovalent interactions between ORC and CIT fragments. It is possible that the number and strength of noncovalent interactions will decrease with the increase in temperature. Consequently, this leads to the weaker binding between ORP and CIT fragments and the increased distance between them. Increased distance between ORP and CIT fragments may be responsible for the sudden drop in density values.

Patchdock online server was used to conduct a docking study to better understand the molecular interaction between ODC and 1JS3 [61-63] which gives reasonable values of global and atomic contact energies as -51.73 and -17.75 kcal/mol. *In-silico* biological screening of ODC against 1JS3 shows various intermolecular interactions which elaborates the potential of ODC on the selected microorganism. ODC contains both an acidic and basic moieties which was bonded through strong intermolecular hydrogen bonding interaction. The elastic nature of the compound allows the transport of electron through hydrogen bonding and made a strong interaction profile with target. ODC docking against 1JS3 demonstrates a significant intermolecular H-bond between the NH site of his510 and O atom of acidic group

of ODC (N-H…O, 2.26Å), O atom of THR508 with H2 atom of acid moiety with a distance of 2.80 Å and a distance of 1.89 Å by O...H-O intermolecular interaction (O atom of LYS with H1 atom of acidic group). Similarly, basic moiety of ODC have twin phenyl ring and along with dimethyl amino system which enhances the bonding between drug and target. There are n number π-alkyl interactions were observed. Strong interaction between proposed drug and π system of PHE568 exhibits a distance of 3.57Å has been observed. On the other hand an enormous number of alkyl system of LEU575, VAL555 and CYS558 interacted with π moiety of ODC through various C-H... π intermolecular interactions with a distances of 4.31 Å, 4.84 Å and 4.59 Å, respectively (Figure S3). Based on the in silico data, ODC appears to be more effective on 1JS3.
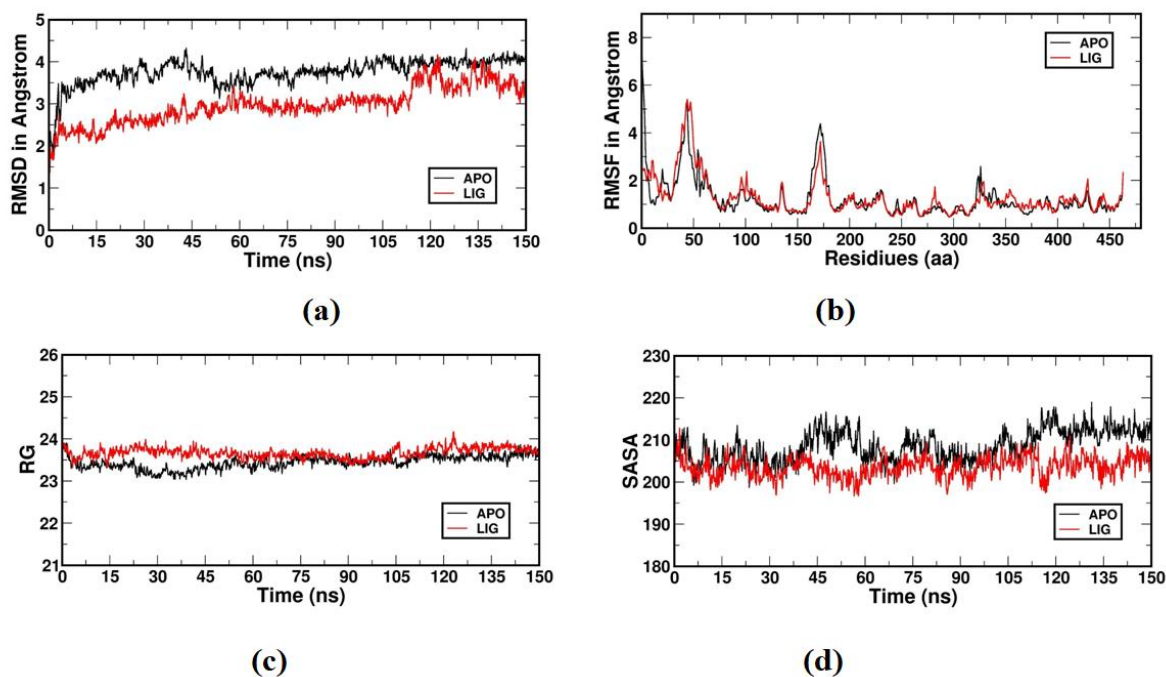

Figure 8. (a) RMSD (b) RMSF (c) Rg (d) SASA of ODC-1JS3 complex

1JS3 and complexes with ODC were subjected to MD simulation for 150 ns, to understand the stability of ODC-1JS3 complex RMSD, RMSF and Hydrogen bonds. For determining the discrepancies between the two conformations, the RMSD is a crucial quantity. The greater in the variance, gives higher RMSD and are determined using a 20 to 150 ns simulation time scale (Fig.8a). During the 150ns simulation, the 1JS3 and complexes were shown to be equilibrated after 20 ns. The average RMSDs for 1JS3 and 1JS3-ODC complex from 20 to 150 ns were 3.5 and 2.8, respectively. Throughout the simulation, these RMSD indicate stability of 1JS3 and ODC complex. Furthermore, the complexes remained stable over the course of the simulation. In RMSF plots, the amino acids responsible in bringing about the overall deviation are investigated [64]. RMSF determines which amino acids in the protein create more vibrations, resulting in protein instability. Fig.8b shows RMSF data for 1JS3 and 1JS3-ODC complex. The Rg gives protein's compactness and was used to check the folding and unfolding of 1JS3 and its complex with ODC. The average Rg. for 1JS3 and ODC complexes from 0 to 150 ns was 23.5 Å and 24.2 Å, respectively shown in

Fig.8c [65]. To comprehend the modulation of inhibitors on the protein, SASA affect the compactness of the protein and in the present case, SASA values were quite small (Fig.8d). The H-bonds stabilize 1JS3-ODC complex and confirm the hydrogen bonds in the docking study. H-Bond result of the 1JS3-ODC complex which shows multiple bonds between the interacting residues and the ODC, where maximum contacts are H-bond based along with water bridges (Fig.S4). An effective protein ligand assembly substantially promotes the creation of a stable complex by combining all of the interactions in the active site. A successful protein-ligand assembly predicts a stable complex formation, given all of the interactions in the active site. To further validate our findings, biochemical, cell-culture-based and animal research will be required [66, 67].

Conclusion

The fundamental normal modes of frequencies are assigned from the experimental and theoretical data. Reactivity of the ODC is identified by means, of ALIE, MEP and FMOs plots. The obtained MEP and ALIE surfaces show that the citrate fragment possesses higher electron density, as the lowest MEP values are mainly localized at its oxygen atoms. ALIE surface revealed that the ORP fragment could be more sensitive toward electrophilic attacks. MD simulations in different solvents show that the fluctuation indicates significant stability in the biological system. During the 150ns simulation, it was found that the 1JS3 and its complex with ODC are equilibrated after 20ns of time. The average RMSDs are between 3.5 and 2.8 (20 ns to 150ns range) and average radius of gyration is 23.5 to 24.2 Å (o to 150 ns) for the 1JS3-ODC complex giving stable complex formation.. RDF calculated after MD simulation showed that H47 atom has the most substantial interactions with the water molecules. Temperature dependence of density indicates a significant drop in the density from 323 K to 343 K.

Acknowledgments

References

[1]   H.S. Akshatha, B.M. Gurupadayya, P.P. Raikar, Validated method for the simultaneous estimation of orphenadrine citrate and paracetamol in tablets by simultaneous equation method, Int. J. ChemTech. Res. 11 (2018) 45-55. https://doi.org/10.20902/IJCTR.2018.110706

[2]   J.F. Desaphy, A. Dipalma, M. De Bellis, T. Costanza, C. Gaudioso, P. Delmas, A.L. George Jr, D.C. Camerino, Involvement of voltage-gated sodium channels blockade in the analgesic effects of orphenadrine, Pain 142 (2009) 225-235, https://doi.org/10.1016/j.pain.2009.01.010

[3]   D.R. Guay, Are there alternatives to use of quinine to treat nocturnal leg cramps?, Consult Pharm. 23 (2008) 141-156, https://doi.org/10.4140/tcp.n.2008.141

[4]   S. Abd-Elsalam, S. Ebrahim, S. Soliman, W. Alkhalawany, A. Elfert, N. Hawash, M. Elkadeem, R. Badawi, Orphenadrine in treatment of muscle cramps in cirrhotic patients; a randomized study, Eur. J. Gastroenterol. Hepatol. 32 (2019) 1042-1045, https://doi.org/10.1097/MEG.0000000000001622

[5]   K.Y. Cheah, K.Y. Mag, L.H. Pang, S.M. Ng, J.W. Wong, S.S. Tan, H.Z. Tan, K.H. Yuen, A randomized single dose, two period crossover bioequivalence study of two fixed dose paracetamol/orphenandrine combination preparations in healthy volunteers

under fasted condition, BMC Pharmacol. Toxicol. 21 (2020) 45. https://doi.org/10.1186/s40360-020-00416-3

[6]   E. Valtonen, A controlled clinical trial of chlormezanone, orphenadrine, orphendrinel paracetamol and placebo in the treatment of painful skeletal muscle spasm, Ann. Clin. Res. 7 (1975) 85-88, PMID: 1103709

[7]   D.N. Haj-Ali, I.I. Hamdan, Development of a capillary electrophoresis method for the determination of orphenadrine citrate in tablets in the presence of paracetamol, Saudi Pharm. J. 18 (2010) 233-237. https://doi.org/10.1016/j.jsps.2010.07.007

[8]   R. Capmana, G. Mangiaterra, M. Tiboni, E. Frangipani, F. Biavasco, S. Lucarini, B. Citterio, A fluorinated analogue of marine bisindole alkaloid 2,2-bis(6-bromo-1H-indol-3-yl)ethanamine as potential anti-biofilm agent and antibiotic adjuvant against staphylococcus aureus, Pharmaceuticals 13 (2020) 210. https://doi.org/10.3390/ph13090210

[9]   K.R. Jeyashri, E. Dhineshkumar, G. Logeshwari, E. Enbaraj, V.J. Ramyadevi, H. Manikandana, M. Sreenivasan, V. Rajathi, J. Chakkaravarthy, R. Govindaraju, Design, synthesis of E-N-substituted-dichlorobenzylidene-2-(pyrrolidin-1-yl)ethanamine Schiff bases derivative and their DFT studies, Mater. Sci. Eng. 1070 (2021) 012015. https://doi.org/10.1088/1757-899X/1070/012015

[10]   M.E. Liechti, Novel psychoactive substances (designer drugs): Overview and pharmacology of modulators of monoamine signaling, Swiss Med. Wkly. 145 (2015) 1-12, https://doi.org/10.4414/smw.2015.14043

[11]   M.R. Braden, J.C. Parrish, J.C. Naylor, D.E. Nichols, Molecular interaction of serotonin 5-HT 2A receptor residues phenethylamine agonists Phe339(6.51) and Phe340(6.52) with superpotent N-benyl phenethylamine agonists, Mol. Pharmacol, 70 (2006) 1956-1964, https://doi.org/10.1124/mol.106.028720.delics

[12]   M. Terrazas-Lopez, N. Lobo-Galo, L.G. Aguirre-Reyes, I. Bustos-Jaimes, J.A. Marcos-Viquez, L. Gonzalez-Segura, A.G. Diaz-Sanchez, Interaction of N-succinyl diamonpimelate descuccinylase with orphenadrine and disulfiram, J. Mol. Struct. 1222 (2020) 128928, https://doi.org/10.1016/j.molstruc.2020.128928

[13]   P. Gjerden, L. Slordal, J.G. Bramness, The use of antipsychotic and anticholinergic antiparkinson drugs in Norway after the withdrawl of orphenadrine, Br. J. Clin. Pharmacol. 68 (2009) 238-242, https://doi.org/10.1111/j.1365-2125.2009.03446.x

[14]   M.H. Cheng, E. Block, F. Hu, M.C. Cobanoglu, A. Sorking, I. Bahar, Insights into the modulation of dopamine transporter function by amphetamine, orphenadrine and cocaine binding, Front. Neurol. 6 (2015)134, https://doi.org/10.3389/fneur.2015.00134

[15]   M.A. El-Nakeeb, H.M. Abou-Shleib, A.M. Khalil, H.G. Omar, O.M. El-Halfawy, In vitro antibacterial activity of some antihistaminics belonging to different groups against multi-drug resistant clinical isolates, Brazilian J. Microbiol. 42 (2011) 980-991, https://doi.org/10.1590/s1517-83822011003000018

[16]   H.S. Maji, S. Maji, M. Bhattacharya, An exploratory study on the antimicrobial activity of cetirizine dihydrochloride, Indian J. Pharm. Sci. 79 (2017) 751-775, https://doi.org/10.4172/pharmaceutical-sciences.1000288

[17]   P. Bruer, P. Hagedorn, M. Kietzmann, A.F. Tohamy, V. Filor, E. Schultz, S. Mielke-Kuschow, J. Meissner, Histamine H1 receptor antagonists enhance the efficacy of antibacterials against Escherichia coli, BMC Vet. Res. 15 (2019) 55, https://doi.org/10.1186/s12917-019-1797-9

[18] N. Escudero, L. Morandeira, M.A. Sanroman, F.J. Deive, A. Rodrigues, Salting out potential of cholinium dihydrogen citrate in aqueous solution of triton surfactants, J. Chem. Thermodyn. 118 (2018) 235-243, https://doi.org/10.1016/j.jct.2017.11.019

[19] T.R. Tran, P. Thevenot, D. Gyawali, J.-C. Chiao, L. Tang, J. Yang, Synthesis and characterization of a biodegradable elastomer featuring a dual crosslinking mechanism, Soft Matter 6 (2010) 2449-2461, https://doi.org/10.1039/C001605E

[20] T.K.A. Sha, M.A. Khan, M.A. Jan, M.N. Ashiq. M.A. Zia, Simultaneous femtomolar detection of paracetamol, diclofenac, and orphenadrine using a carbon nanotube/zinc oxide nanoparticle based electrochemical sensor, ACS Appl. Nano Mater. 4 (2021) 4699-4712, https://doi.org/10.1021/acsanm.1c00310

[21] S. Seshadri, S. Gunasekaran, S. Muthu, S. Kumaresan, R. Arunbalaji, Vibrational spectroscopy investigation using ab initio and density functional theory on flucytosine, J. Raman Spectrosc. 38 (2007) 1523-1531, https://doi.org/10.1002/jrs.1808

[22] S. Gunasekarana, S. Seshadri, S. Muthu, S. Kumaresan, R. Arunbalaji, Vibrational spectroscopy investigation using ab initio and density functional theory on p-anisaldehyde, Spectrochim. Acta 70 (2008) 550-556, https://doi.org/10.1016/j.saa.2007.07.050

[23] M. Kaur, J.P. Jasinski, A.C. Keelye, H.S. Yathirajan, B.P. Siddaraju, Orphenadrinium dihydrogen citrate, Acta Cryst. E69 (2013) o248, https://doi.org/10.1107/s1600536813001207

[24] L.G. Ferreira, R.N.D. Sanbtos, G. Oliva, A.D. Andricopulo, Molecular docking and structure based drug design strategies, Molecules 24 (2015) 13384-13421, https://doi.org/10.3390/molecules200713384

[25] Y. Cai, N.K. Yilmaz, W. Myint, R. Ishima, C.A. Schiffer, Differential flap dynamics in wild-type and a drug resistant variant of HIV-1 protease revealed by molecular dynamics and NMR relaxation, J. Chem. Theory Comput. 8 (2012) 3452-3462, https://doi.org/10.1021/ct300076y

[26] M.D. Tiezza, F.M. Bickelhaupt, L. Flohe, L. Orian, Proton transfer and SN2 reactions as steps of fast selenol and thiol oxidation in proteins: a model molecular study based on GPx, ChemPlusChem 86 (2021) 524, https://doi.org/10.1002/cplu.202000781

[27] W. Xie, T. Li, C. Chen, H. Wu, S. Liang, H. Chang, B. Liu, E. Drioli, Q. Wang, J.C. Crittenden, Using the green solvent dimethyl sulfoxide to replace traditional solvents partly and fabricating PVC/PVC-g-PEGMA blended ultrafiltration membranes with high permeability and rejection, Ind. Eng. Chem. Res. 58 (2019) 6413-6423, https://doi.org/10.1021/acs.iecr.9b00370

[28] S.Geethaa, P.J.Thavamany, S.P.Chiew, O.M.Thong, Interference from ordinarily used solvents in the outcomes of artemia salina lethality test, J. Adv. Pharm. Technol. Res. 4 (2013) 179-182, https://doi.org/10.4103/2231-4040.121411

[29] Gaussian 16, Revision A.03, M.J. Frisch, G.W. Trucks, H.B. Schlegel, G.E. Scuseria, M.A. Robb, J.R. Cheeseman, G. Scalmani, V. Barone, G.A. Petersson, H. Nakatsuji, X. Li, M. Caricato, A.V. Marenich, J. Bloino, B.G. Janesko, R. Gomperts, B. Mennucci, H.P. Hratchian, J.V. Ortiz, A.F. Izmaylov, J.L. Sonnenberg, D. Williams-Young, F. Ding, F. Lipparini, F. Egidi, J. Goings, B. Peng, A. Petrone, T. Henderson, D. Ranasinghe, V.G. Zakrzewski, J. Gao, N. Rega, G. Zheng, W. Liang, M. Hada, M. Ehara, K. Toyota, R. Fukuda, J. Hasegawa, M. Ishida, T. Nakajima, Y. Honda, O. Kitao, H. Nakai, T. Vreven, K. Throssell, J.A. Montgomery, Jr., J.E. Peralta, F.

Ogliaro, M.J. Bearpark, J.J. Heyd, E.N. Brothers, K.N. Kudin, V.N. Staroverov, T.A. Keith, R. Kobayashi, J. Normand, K. Raghavachari, A.P. Rendell, J.C. Burant, S.S. Iyengar, J. Tomasi, M. Cossi, J.M. Millam, M. Klene, C. Adamo, R. Cammi, J.W. Ochterski, R.L. Martin, K. Morokuma, O. Farkas, J.B. Foresman, D.J. Fox, Gaussian, Inc., Wallingford CT, 2016.

[30] GaussView, Version 6.1, R. Dennington, T.A. Keith, J.M. Millam, Semichem Inc., Shawnee Mission, KS, 2016.

[31] P. Burkhard, P. Dominici, C. Borri-Voltattomi, J.N. Jansonius, V.N. Malashkevic, Structural insight into Parkinson's disease treatment from drug-inhibited DOPA decarboxylase, Nature Struct. Biol. 8 (2001) 963-967, https://doi.org/10.1038/nsb1101-963

[32] E. Chow, C.A. Rendleman, K.J. Bowers, R.O. Dror, D.H. Hughes, J. Gullingsrud, F.D. Sacerdoti, D.E. Shaw, Desmond performance on a cluster of multicore processors (DE Shaw Research Report), DESRES/TR-2008-01.

[33] K.J. Bowers, D.E. Chow, H. Xu, R.O. Drora, M.P. Eastwood, B.A. Gregersen, J.L. Klepeis, I. Kolossvary, M.A. Moraes, F.D. Sacerdoti, J.K. Salmon, Scalable algorithms for molecular dynamics simulations on commodity clusters, in: SC'06: Proceedings for the 2006 ACM/IEEE Conference on Supercomputing 2006 Nov 11 (pp.43-43), IEEE.

[34] A.D. Bochevarov, E. Harder, T.F. Hughes, J.R. Greenwood, D.A. Braden, D.M. Philipp, D. Rinaldo, M.D. Halls, J. Zhang, R.A. Friesner, Jaguar: A high-performance quantum chemistry software program with strengths in life and materials sciences, Int. J. Quantum Chem. 113 (2013) 2110-2142, https://doi.org/10.1002/qua.24481

[35] L.D. Jacobson, A.D. Bochevarov, M.A. Watson, T.F. Hughes, D. Rinaldo, S. Ehrlich, T.B. Steinbrecher, S. Vaitheeswaran, D.M. Philipp, M.D. Halls, Automated transition state search and its application to diverse types of organic reactions, J. Chem. Theory Comput. 13 (2017) 5780-5797, https://doi.org/10.1021/acs.jctc.7b00764

[36] Schrodinger Release 2021-4: Desmond Molecular Dynamics System, D.E. Shaw Research, New York, NY, 2021, Maestro-Desmond Interoperability Tools, Schrodinger, New York, NY, 2021., (n.d.).

[37] Schrodinger Release 2021-4: Jaguar, Schrodinger, LLC, New York, NY, 2021.

[38] D. Shivakumar, J. Williams, Y. Wu, W. Damm, J. Shelley, W. Sherman, Prediction of absolute salvation free energies using molecular dynamics free energy perturbation and the OPLS force field, J. Chem. Theor. Comput. 6 (2010) 1509-1519, https://doi.org/10.1021/ct900587b

[39] E. Harder, W. Damm, J. Maple, C. Wu, M. Reboul, J.Y. Xiang, L. Wang, D. Lupyan, M.K. Dahlgren, J.L. Knight, OPLS3; a force field providing broad coverage of drug-like small molecules and proteins, J. Chem. Theor. Comput. 12 (2015) 281-296, https://doi.org/10.1021/acs.jctc.5b00864

[40] W.L. Jorgensen, D.S. Maxwell, J. Tirado-Rives, Development and testing of the OPLS all-atom force field on conformational energetic and properties of organic liquids, J. Am. Chem. Soc. 118 (1996) 11225-11236, https://doi.org/10.1021/ja9621760

[41] W.L. Jorgensen, J. Tirado-Rives, The OPLS [optimized potentials for liquid simulations] potential functions for proteins, energy minimizations for crystals of cyclic peptides and crambin, J. Am. Chem. Soc. 110 (1988) 1657-1666, https://doi.org/10.1021/ja00214a001

[42]   A.D. Becke, Density functional thermochemistry. III. The role of exact exchange, J. Chem. Phys. 98 (1993) 5648-5652, https://doi.org/10.1063/1.464913

[43]   P.C. Hariharan, J.A. Pople, The influence of polarization functions on molecular orbital hydrogenation energies, Theor. Chim. Acta 28 (1973) 213-222, https://doi.org/10.1007/BF00533485

[44]   W.J. Hehre, R. Ditchfield, J.A. Pople, Self-consistent molecular orbital methods. XII. Further extensions of Gaussian-type basis sets for use in molecular orbital studies of organic molecules, J. Chem. Phys. 56 (1972) 2257-2261, https://doi.org/10.1063/1.1677527

[45]   R. Ditchfield, W.J. Hehre, J.A. Pople, Self-consistent molecular orbital methods. IX. An extended Gaussina-type basis for molecular-orbital studies of organic molecules, J. Chem. Phys. 54 (1971) 724-728, https://doi.org/10.1063/1.1674902

[46]   S.T. Schneebeli, A.D. Bochevarov, R.A. Friesner, Parametrization of a B3LYP specific correction for noncovalent interactions and basis set superposition error on a gigantic data set of CCSD(T) quality noncovalent interaction energies, J. Chem. Theory Comput. 7 (2011) 658-668, https://doi.org/10.1021/ct100651f

[47]   C.J.Cramer, D.G.Truhlar, Implicit solvation models: equilibria, structure, spectra, and dynamics, Chem. Rev. 99 (1999) 2161-2200, https://doi.org/10.1021/cr960149m

[48]   N.P.G. Roeges, A guide to the complete interpretation of infrared spectra of organic structures, New York, NY, John Wiley and Sons Inc., 1994.

[49]   A.S. El-Azab, Y.S. Mary, C.Y. Panicker, A.A.-M. Abdel-Aziz, I.A. Al-Suwaidan, C. Van Alsenoy, FT-IR, FT-Raman and molecular docking study of ethyl 4-(2-(4-oxo-3-phenethyl-3,4-dihydroquinazolin-2-ylthio)acetamido)benzoate, J. Mol. Struct. 1111 (2016) 9-18, https://doi.org/10.1016/j.molstruc.2016.01.041

[50]   V.V. Aswathy, S. Alper-Hayta, G. Yalcin, Y.S. Mary, C.Y. Panicker, P.J. Jojo, F. Kaynak-Onurdag, S. Armakovic, S.J. Armakovic, I. Yildiz, C. Van Alsenoy, Modification of benzoxazole derivative by bromine-spectroscopic, antibacterial and reactivity study using experimental and theoretical procedures, J. Mol. Struct. 1141 (2017) 495-511, https://doi.org/10.1016/j.molstruc.2017.04.010

[51]   A.S. El-Azab, Y.S. Mary, Y.S. Mary, C.Y. Panicker, A.A.-M. Abdel-Aziz, M.A. El-Sherbeny, S. Armakovic, S.J. Armakovic, C.Van Alsenoy, Newly synthesized dihydroquinazoline derivative from the aspect of combined spectroscopic and computational study, J. Mol. Struct. 1134 (2017) 814-827, https://doi.org/10.1016/j.molstruc.2017.01.044

[52]   A.S. El-Azab, Y.S. Mary, Y.S. Mary, C.Y.Panicker, A.A.-M. Abdel-Aziz, M.A. Mohamed, S. Armakovic, S.J. Armakovic, C. Van Alsenoy, Spectroscopic and reactive properties of a newly synthesized quinazoline derivative: Combined experimental, DFT, molecular dynamics and docking study, J. Mol. Struct. 1134 (2017) 863-881, https://doi.org/10.1016/j.molstruc.2017.01.032

[53]   Y.S. Mary, M.M. Al-Shehri, K. Jalaja, F.A.M. Al-Omary, A.A. El-Emam, C.Y. Panicker, S. Armakovic, S.J. Armakovic, O. Temiz-Arpaci, C. Van Alsenoy, Synthesis, vibrational spectroscopic investigations, molecular docking, antibacterial studies and molecular dynamics study of 5-[(4-nitrophenyl)acetamido]-2-(4-tert-butylphenyl)benzoxazole, J. Mol. Struct. 1133 (2017) 557-573, https://doi.org/10.1016/j.molstruc.2016.12.020

[54] N.D. Ojo, R.W. Krause, N.O. Obi-Egbedi, Electronic and nonlinear optical properties of 3-(((2-substituted-4-nitrophenyl)imino)methyl)phenol, Comput. Theor. Chem. 1192 (2020) 113050, https://doi.org/10.1016/j.comptc.2020.113050

[55] S. Muthu, G. Ramachandran, Spectroscopic studies (FTIR, FT-Raman and UV-Visible), normal coordinate analysis, NBO analysis, first order hyper polarizability, HOMO and LUMO analysis of (1R)-N-(prop-2-yn-1-yl)-2,3-dihydro-1H-inden-1-amine molecule by ab initio HF and density functional methods, Spectrochim. Acta 121 (2014) 394-403, https://doi.org/10.1016/j.saa.2013.10.093

[56] R.G. Parr, L.V. Szentpaly, S. Liu, Electrophilicity index, J. Am. Soc. Chem. 121 (1999) 983494, https://doi.org/10.1021/ja983494x

[57] S. Demir, F. Tinmaz, N. Dege, I.O. Ilhan, Vibrational spectroscopic studies, NMR, HOMO-LUMO, NLO and NBO analysis of 1-(2-nitrobenzyl)-3,5-diphenyl-4,5-dihydro-1H-pyrazole with use X-ray diffractions and DFT calculations, J. Mol. Struct. 1108 (2016) 637-648, https://doi.org/10.1016/j.molstruc.2015.12.057

[58] A.E. Reed, F. Weinhold, F. Weinhold, Natural localized molecular orbitals, J. Chem. Phys. 83 (1985) 1736, https://doi.org/10.1063/1.449360

[59] Y.S. Mary, K. Raju, C.Y. Panicker, A.A. Al-Saadi, T. Thiemann, Molecular conformational analysis, vibrational spectra, NBO analysis and first hyperpolarizability of (2E)-3-(3-chlorophenyl)prop-2-enoic anhydride based on density functional theory calculations, Spectrochim. Acta 131 (2014) 471-483, https://doi.org/10.1016/j.saa.2014.04.111

[60] T. Pooventhiran, U. Bhattacharyya, D.J. Rao, V. Chandramohan, P. Karunakar, A. Irfan, Y.S. Mary, R.Thomas, Detailed spectra, electronic properties, qualitative non-covalnet interaction analysis, solvatochromism, docking and molecular dynamics simulations in different solvent atmosphere of cenobamate, Struct. Chem. 31 (2020) 2475-2485, https://doi.org/10.1007/s11224-020-01607-8

[61] https://bioinfo3d.cs.tau.ac.il>Patchdock

[62] J.S. Al-Otaibi, Y.S. Mary, Computational studies, GERS, photovoltaic modeling and molecular docking studies of diethylstilbestrol and its methyl ether, Polycyclic Aromatic Compounds (2022), https://doi.org/10.1080/10406638.2022.2038219

[63] D. Schneidman-Duhovny, Y. Inbar, R. Nussiov, H.J. Wolfson, Patchdock and Symmdock: servers for rigid and symmetric docking, Nucl. Acids Res. 33 (2005) W363-367, https://doi.org/10.1093/nar/gki481 .

[64] J.S. Al-Otaibi, Y.S. Mary, Y.S. Mary, R. Yadav, Structural and reactivity studies of pravadoline-An ionic liquid, with reference to its wavefunction-relative properties using DFT and MD simulation, J. Mol. Struct. 1245 (2021) 131074, https://doi.org/10.1016/j.molstruc.2021.131074

[65] Y.S. Mary, Y.S. Mary, A.S. Rad, R. Yadav, I. Celik, S. Sarala, Theoretical investigation on the reactive and interaction properties of sorafenib-DFT, AIM, spectroscopic and Hirshfeld analysis, docking and dynamics simulations, J. Mol. Liquid. 330 (2021) 115652, https://doi.org/10.1016/j.molliq.2021.115652

[66] Y.S. Mary, Y.S. Mary, S. Armakovic, S.J. Armakovic, R. Yadav, I. Celik, P. Mane, B. Chakraborty, Stability and reactivity study of bio-molecules brucine and colchicines towards electrophile and nucleophile attacks: Insight from DFT and MD simulations, J. Mol. Liquid. 335 (2021) 116192, https://doi.org/10.1016/j.molliq.2021.116192
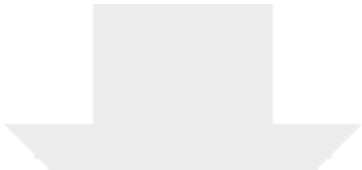
[67]   M. Smitha, Y.S. Mary, Y.S. Mary, G. Serdaroglu, P. Chowdhury, M. Rana, H. Umamahesvari, B.K. Sarojini, B.J. Mohan, R. Pavithran, Modeling the DFT structural reactivity studies of a pyrimidine-6-carboxylate derivative with reference to its wavefunction-dependent, MD simulations and evaluation for potential antimicrobial activity, J. Mol. Struct. 1237 (2021) 130397, https://doi.org/10.1016/j.molstruc.2021.130397

Declaration of Competing Interest

The authors declare no conflict of interest.

Author contribution statement

All authors: Conceptualization, Methodology, Data curation, Writing, Software, Validation.

Click here to access/download
Supplementary Material
SI.docx